Hyperspectral Imaging with Stimulated Raman Scattering by Chirped Femtosecond Lasers

Hyperspectral Imaging with Stimulated Raman Scattering by Chirped Femtosecond Lasers

Dan Fu[1], Gary Holtom[1], Christian Freudiger[1], Xu Zhang[1,2], Xiaoliang Sunney Xie[1,]*

Department of Chemistry and Chemical Biology, Harvard University

School of Engineering and Applied Sciences, Harvard University

ABSTRACT: Raman microscopy is a quantitative, label-free and noninvasive optical imaging technique for studying inhomogeneous systems. However, the feebleness of Raman scattering significantly limits the use of Raman microscopy to low time resolutions and primarily static samples. Recent developments in narrowband stimulated Raman Scattering (SRS) microscopy have significantly increased the acquisition speed of Raman based label-free imaging by a few orders of magnitude, at the expense of reduced spectroscopic information. Based on a spectral focusing approach, we present a fast SRS hyperspectral imaging system using chirped femtosecond lasers to achieve rapid Raman spectra acquisition while retaining the full speed and image quality of narrowband SRS imaging. We demonstrate that quantitative concentration determination of cholesterol in the presence of interfering chemical species can be achieved with sensitivity down to 4 mM. For imaging purposes, hyperspectral imaging data in the C-H stretching region is obtained within a minute. We show that mammalian cell SRS hyperspectral imaging reveals the spatially inhomogeneous distribution of saturated lipids, unsaturated lipids,

cholesterol and protein. The combination of fast spectroscopy and label-free chemical imaging will enable new applications in studying biological systems and material systems.

KEYWORDS: Raman spectroscopy, Stimulated Raman scattering microscopy, Raman spectroscopic imaging

INTRODUCTION

Raman spectroscopy is extremely powerful for charactering materials through their intrinsic molecular vibrational contrasts. This capability, when extended to microscopy, becomes especially useful for investigating spatially inhomogeneous specimens. With the availability of commercial confocal Raman microscopy systems in recent years, the method has been increasingly used to study biological samples [1-3]. With few exceptions, spontaneous Raman scattering is severely limited by low signal intensity, and acquiring a two dimensional Raman map of a biological sample could take a fraction of an hour to complete, hindering its utility for the study of dynamic processes, especially those happening in living biological systems. Coherent anti-Stokes Raman scattering (CARS) microscopy has been developed over the past decade to address this problem [4,5]. CARS makes use of two pulsed laser beams with an energy difference tuned to the vibrational frequency of the molecule of interests to obtain much stronger vibrational signals at the anti-Stokes frequency. When applied to the high wavenumber region (CH_2 and CH_3 stretching modes) of biological specimens, video-rate imaging can be achieved with good signal-to-noise ratio (SNR) [6]. In order to obtain spectroscopic information, multiplex CARS can be employed, where both a picosecond narrowband laser and a femtosecond broadband laser are used. The narrowband laser determines spectral resolution and the broadband laser determines the spectral bandwidth [7-10]. The imaging speed is generally limited by

the readout speed of the CCD detector to 10-100ms per pixel. It is also possible to use narrowband CARS and sweep the resonance frequency, which can achieve 1 sec/frame imaging speed[11,12]. This method typically requires mechanical tuning of an optical parametric oscillator (OPO) and only a limited range can be scanned without time-consuming adjustments. The third approach uses two synchronized broadband lasers and the Raman spectrum is acquired by scanning the time delay between the two lasers when they are appropriately chirped. This is known as the spectral focusing approach[13]. It has the advantage of tunable spectral resolution and a simple scanning mechanism. However, all approaches based on CARS have a well-known non-resonant background problem that distorts vibrational spectra and causes image artifacts[5]. The nonlinear dependence of the CARS signal on chemical concentration also significantly hinders the quantitative analysis of chemical composition. Although phase retrieval using the maximum entropy method or the Kramers-Kronig method allows reconstruction of real Raman spectra [14], the analysis process is complicated and it has not been shown that individual spatially and spectrally overlapping chemical components in a complex sample can be quantified using this approach.

In recent years, stimulated Raman scattering (SRS) microscopy has emerged as an alternative to CARS microscopy that is free from the aforementioned issues [15-18]. SRS eliminates the non-resonant background problem because the generated third order SRS nonlinear polarization is directly heterodyne mixed and amplified by the input beam with the exact same phase, therefore always resulting in a zero non-resonant contribution. Consequently, the spectral shape of SRS is identical to that of spontaneous Raman, allowing straightforward comparison. Moreover, the SRS signal has a linear dependence on the chemical concentration, allowing for simple quantitative analysis. These capabilities have facilitated applications in many different research

areas such as lipidomics, pharmacokinetics, biofuel production, and cancer detection [16,19,20]. Typical SRS microscopy uses synchronized picosecond lasers with narrow bandwidth (<10cm^{-1}) to excite the sample, thereby acquiring Raman information on a specific predetermined Raman band. To obtain information on a different Raman band, one of the lasers has to be tuned to a different wavelength, which typically involves either cavity length change or crystal temperature change or both [21]. This spectral scanning process is usually slow and susceptible to the optical power drift and wavelength drift. It is also possible to employ a picosecond and femtosecond laser source to acquire spectroscopic information in a manner similar to multiplex CARS microscopy [22,23]. However, SRS microscopy uses a high frequency lock-in amplifier and a multiplex detection approach that requires a lock-in amplifier array, which is difficult with current technology. Recent developments in our group used spectrally-tailored or multiplex excitation to achieve molecular selectivity [24,25]. Those approaches work well for simple systems in which all the component spectra are well characterized, but the instrumentation is complicated and has limited sensitivity. Most recently, SRS spectroscopy and imaging using the spectral focusing approach has also been demonstrated by using a femtosecond oscillator and a fiber-generated secondary source[26,27]. It allows acquisition of reliable Raman spectrum over a large spectral range. However, the low power output and large bandwidth mismatch between the pump and the Stokes significantly limits the imaging speed to ms/pixel.

In this manuscript, we present SRS hyperspectral imaging using the spectral focusing approach, which improves the imaging speed of the previous works by a thousand fold. We present SRS spectra imaging of a bead mixture as well as biological cells that is orders of magnitude faster than confocal Raman and multiplex CARS while obtaining reliable Raman spectra in the CH stretching region. We demonstrate that the chemical concentration of spectrally

overlapping species can be determined with sensitivity and accuracy down to a few millimolar. We further demonstrate that with a nonnegative least square algorithm, SRS hyperspectral imaging provides detailed chemical mapping of several species in fixed mammalian cells. We believe the flexibility of choice among fast spectroscopy, single band imaging and hyperspectral imaging provides an extremely powerful tool for studying material and biological systems that is unparalleled by either spontaneous Raman or previous CARS/SRS imaging approaches.

THEORETICAL BACKGROUND

In the most common case of SRS spectroscopy using synchronized picosecond pulses, the spectroscopic resolution is determined by the bandwidth of the two lasers. If transform-limited femtosecond pulses are used instead, the signal size increases at the expense of reduced spectral resolution [28,29]. In order to resolve the conflict of narrow spectral resolution and large spectral bandwidth, chirped pulse excitation known as spectral focusing has been developed for CARS microscopy [13,30-33]. Most recently, similar approaches have been used in SRS for spectroscopy and hyperspectral imaging[26,27]. The theoretical rationale for SRS and CARS is very similar. When the two input pulses are linearly chirped Gaussian femtosecond pulses (for simplicity, the same chirp and bandwidth parameters are assumed for both pulses), we can express the input electric field as:

$$E = A_1 e^{i(k_1 z - \omega_1 t + \omega_1 t_0)} \Big/ \sqrt{\tau}\, e^{-(t-t_0)^2/2\tau^2} e^{-ib(t-t_0)^2} + A_2 e^{i(k_2 z - \omega_2 t)} \Big/ \sqrt{\tau}\, e^{-t^2/2\tau^2} e^{-ibt^2} + c.c. \quad (1)$$

where A, k, ω, τ, t_0, b represent the amplitude, wavevector, wavenumber, pulse duration, interpulse delay and chirp of the propagating pulses, respectively. Subscript 1 and 2 denotes pump and Stokes pulses, respectively. c.*c*. represents complex conjugate. The excitation efficiency of these two chirped pulses is equivalent to two narrowband transform-limited

picosecond pulses with the same pulse durations. The relationship between chirp parameter b, chirped pulse duration $\Delta\tau$, and chirped pulse bandwidth $\Delta\lambda$ is:

$$b = \sqrt{(\frac{\pi c \Delta\lambda}{\lambda^2 \Delta\tau})^2 - \frac{4(In2)^2}{\Delta\tau^4}} \quad (2)$$

Most importantly, the delay between the pump and Stokes pulse effect a change in the probed Raman oscillation frequency from ω_1-ω_2 to ω_1-ω_2-$2bt_0$, Therefore, SRS hyperspectral imaging can be realized by performing SRS imaging while sequentially sweeping the interpulse delay t_0 between the pump and the Stokes beam. It is worth noting that as t_0 increases, the SRS signal also decreases by a factor of $exp[-(t_0/2\tau)^2]$.

Previous SRS spectral focusing implementations all used supercontinuum generated by a piece of photonic crystal fiber as either the pump or the Stokes beam[26,27]. While this approach only requires one femtosecond laser source and can provide a large spectral bandwidth, it suffers from low signal-to-noise ratio due to two reasons: 1) the pump and Stokes have large bandwidth mismatch; 2) output power from the fiber is limited. As a result, a long pixel dwell time is needed, thus defeating the purpose of fast hyperspectral imaging. For high speed hyperspectral SRS imaging, we propose using a broadband femtosecond oscillator and an optical parametric oscillator as Stokes and pump beam, respectively. In the case of imaging in the fingerprint region, it is also possible to derive both beams from a single high power ultra-broadband Ti:sapphire femtosecond laser [33].

EXPERIMENTAL SECTION

SRS spectroscopy An ultra-broadband Ti: sapphire laser (MICRA from Coherent) is used to demonstrate high resolution SRS spectroscopy. Figure 1(A) shows our experimental setup. The

MICRA provides an output spectrum spanning from 750 to 850 nm (at FWHM). Using two dichroic filters SP800 and LP820 (Chroma Technology), the spectrum can be sliced into two portions: one is from 740 nm - 790 nm and is modulated by an electro-optical modulator (EOM) at 5 MHz, serving as the pump beam; the other portion is from 810 nm – 870 nm and is unmodulated, serving as the Stokes beam. A motorized delay line is inserted into the Stokes beam to scan the delay between the two pulse trains. Both beams are chirped by a 3cm long high dispersion NSF57 glass block [32]. Additional 1.5 cm long NSF57 glass as well as a 2 cm AOM crystal is placed in the Stokes beam path to adjust the chirp of the two beams to be almost equal. Pulse durations of the pump and Stokes beam are measured to be 2.5 ps and 2.9 ps respectively using an autocorrelator (APE-Berlin). After recombining the two beams on the second dichroic filter, the laser is sent into an inverted microscope (NIKON TE300). The sample is typically an organic liquid sandwiched between two coverglasses using double-sided tape as a spacer. On the detection side, the pump beam is filtered out by a long pass filter (RazorEdge 808 nm, Semrock) and the Stokes beam is detected by a 7×6 mm^2 Si photodiode (Advanced Photonix) biased at 50V. The electric signal is filtered by a low pass filter (BLP-5, Minicircuits) and then measured by a RF lock-in amplifier (SRS844, Stanford Research System).

SRS hyperspectral imaging To demonstrate the hyperspectral imaging capability of this method, we adopt another laser system which is composed of a home-built Yb: KGW femtosecond laser and a synchronously green pumped optical parametric oscillator (OPO) [34]. This laser system provides much higher average power than MICRA and allows us to image at high speed the congested CH stretching region (2800-3100 cm^{-1}), where resolving the spectrum is critical for quantitative chemical composition analysis. The two beams are chirped with different lengths of NSF57 glass block and then combined on a dichroic mirror before sending to

a laser scanning microscope (Olympus IX71/FV300). Stokes pulse duration after chirping is 1.8 ps, giving a theoretical maximum resolution of about 10 cm^{-1}. For hyperspectral imaging experiments, the frame trigger of the confocal scanning unit is used to trigger the delay stage movement on the Stokes arm at the start of each frame. We use an Olympus UPLSAPO60X (NA = 1.2) as the focusing objective. Each frame is 512×512 pixels and takes 1.12 second to scan using the fast home-built lock-in amplifier [16]. A XYT scan is used to acquire hyperspectral imaging data, with T corresponding to the pump-Stokes delay (linearly related to Raman frequency).

Polymer bead mixture imaging A mixture of melamine (3 μm, Corpuscular), polystyrene (2 μm, Polysciences) and PMMA (1-10 μm, Polysciences) is prepared by mixing three bead solutions together in a 15 mL conical tube. Agarose (Invitrogen) is then added to the solution to a final concentration of 1% by weight. The solution is vortexed for one minute and heated to 85°C. A drop of solution is placed on a No. 1.5 coverslip and immediately covered by a 1 mm thick cover slide. The prepared sample is used for imaging within 30 minutes.

HeLa cell imaging Live HeLa cells are obtained from ATCC and cultured in Dulbecco's modified eagle medium (DMEM) supplemented with 10% fetal bovine serum (FBS). The cells are passaged, transferred onto a No. 1.5 glass coverslip and then cultured for 12 h before imaging. For fixed cell imaging, the cells are fixed by 4% paraformaldehyde for 20 min. They are then washed and mounted between a coverslip and a cover slide for imaging. For SRS basis spectra calibration, 1,2-dipalmitoyl-*sn*-glycero-3-phosphocholine (DPPC, represents saturated lipids), 1,2-dioleoyl-*sn*-glycero-3-phosphocholine (DOPC, represents unsaturated lipids), and cholesterol are purchased from Avanti Polar Lipids and dissolved in deuterated chloroform at 25% concentration (by weight). Bovine serum albumin (BSA) is purchased from Sigma-Aldrich

and dissolved in deuterated water at 25% concentration (by weight). A drop of each solution is sandwiched between a coverslip and a cover slide for SRS spectroscopy measurement.

RESULTS AND DISCUSSION

SRS spectroscopy of liquids We measure the SRS spectrum of a few different organic liquids by recording the SRS signal from the lock-in amplifier while scanning the interpulse delay between the pump and the Stokes beam derived from a single ultra-broadband Ti: sapphire laser (Figure 1(A)). For comparison, Figure 1(B) shows the spontaneous Raman spectra of acetone, ethanol and oleic acid measured by a commercial confocal Raman instrument (Horiba Jobin Yvon). We first need to convert the optical delay to Raman wavenumber for SRS spectroscopy. Prominent spontaneous Raman peaks of acetone and ethanol are used to calibrate the linear coefficient 2*b*. Linear fitting of these Raman peaks to corresponding optical delays in SRS measurements results in a calibration curve which can be used to determine Raman shift at any interpulse delay (Figure 1(C)). The SRS Raman spectra span the range from 500 cm^{-1} to 2000 cm^{-1}.The lower bound is set by how well the dichroic filters can separate the pump and Stokes beams, and the upper bound is determined by the optical bandwidth of the laser. Figure 1(D) shows the measured SRS spectra from acetone, ethanol and oleic acid. They are almost identical to their spontaneous counterparts except for relative intensity differences at low and high wavenumbers due to decreased pulse overlap. This intensity variation is always constant and can be removed by calibration against samples with known signals if needed (see Supporting Information). The spectral resolution is slightly worse than predicted by theory, because the pulses have significant high order chirp due to their large bandwidths. Nonetheless, we can still roughly resolve the two peaks of ethanol at 1055 and 1090 cm^{-1}, suggesting a spectral resolution

of ~35cm^{-1}. This spectroscopic capability is a significant advantage compared to multiplex CARS, where reliable Raman spectrum cannot be obtained without complicated post-processing [35]. Compared to SRS with synchronized picosecond beams, this method provides convenient and rapid Raman tuning for imaging purposes.

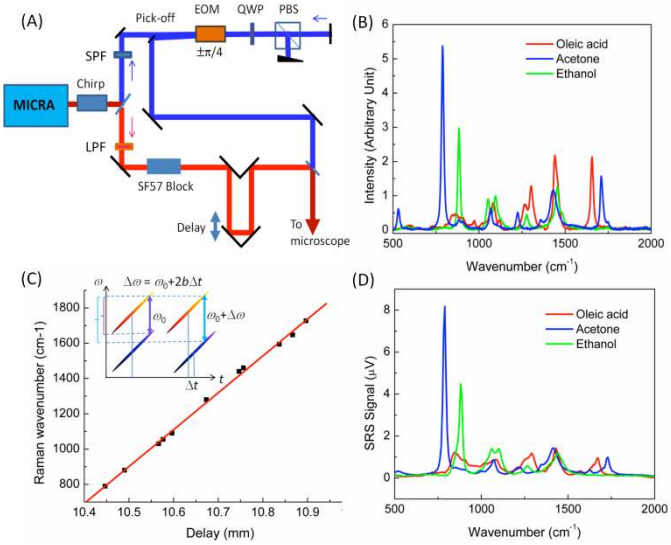

Figure 1: (A) Schematic diagram of SRS spectroscopy setup based on a single ultra-broadband Ti: sapphire laser. SPF: short-pass filter; LPF: long-pass filter; EOM: electro-optical modulator; QWP: quarter waveplate; PBS: polarizing beamsplitter. (B) Spontaneous Raman spectra of oleic acid, acetone and ethanol. (C) Calibration of Raman shift with respect to pump-Stokes pulse delay using a set of Raman peaks of acetone and ethanol; insets showing the schematic diagram illustrating the relationship between Raman shift and interpulse delay; (D) SRS spectroscopy measured by swept-delay chirped femtosecond pulses.

Quantitative determination of chemical concentrations by SRS hyperspectral imaging We first demonstrate that SRS hyperspectral imaging can quantitatively determine chemical concentrations in binary mixture solutions. SRS images are acquired while the interpulse delay is continuously scanned. Two chemicals – oleic acid and cholesterol, with large Raman spectral overlap, are mixed in deuterated chloroform at different concentration ratios. This mimics the

situation of lipid imaging in cells as will be shown later. The oleic acid concentration is fixed at 0.2 mol/L (M) while the cholesterol concentration is varied from 0.2 M to 0.004 M. The calibration spectra are acquired through direct SRS hyperspectral imaging measurements of 0.4 M oleic acid solution and 0.4 M cholesterol solution. SRS spectra are obtained by averaging imaging data from an area of 256×256 pixels in the center for every Raman shift image. Figure 2(A) shows the obtained SRS spectra for all solutions. After least-square linear decomposition, the respective concentration of oleic acid and cholesterol in the mixtures can be extracted. We divide the cholesterol concentration by oleic acid concentration to eliminate errors induced by

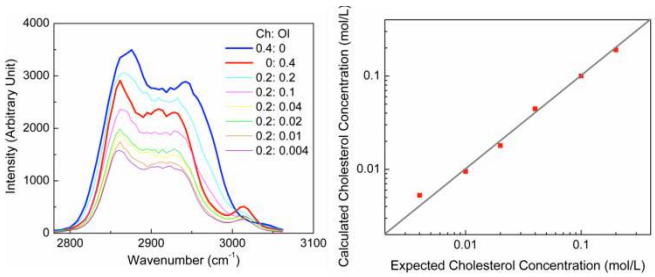

Figure 2: (A) Measured SRS spectra of eight solutions of cholesterol (Ch) and Oleic acid (Ol) mixed at different concentrations (unit mol/L); (B) Calculated cholesterol concentration (red dots) based on SRS spectral decomposition plotted against expected cholesterol concentration (black line).

solvent evaporation and laser power fluctuation. The obtained cholesterol concentration is plotted in Figure 2(B). The calculated values have less than 10% error for a concentration higher than 4 mM in the presence of interfering species with 50 times higher concentration, proving the validity of SRS spectral decomposition for strongly overlapping Raman bands. The linearity of the curve also ensures that no cross-talk in chemical mapping exists in the linear decomposition process, an important characteristic for quantitative chemical imaging. We note that it is not necessary to perform spectral normalization for spectral decomposition purposes because the

sample and calibration solution SRS are measured the same way, cancelling any power-dependent spectral variation.

SRS hyperspectral imaging of polymer bead mixture For spatially inhomogeneous but segregated samples, the calibration spectra can be obtained *in situ*. We show SRS imaging of a mixture of melamine (3μm, Corpuscular), polystyrene (2μm, Polysciences) and PMMA (1-10μm, Polysciences) beads at successive delays for a total of 80 frames with increments of 4.15 cm^{-1}. Figure 3(B) shows an extracted frame at 3028 cm^{-1} with 512×512 pixels. At every single pixel in the frame, a spectrum can be plotted and Figure 3(C) shows three representative spectra for different beads (at the arrow point). For comparison, measured spontaneous Raman spectra of the beads are shown in Figure 3(A). The SRS spectra are consistent at different spatial locations and match spontaneous Raman spectra. We note that the melamine bead SRS spectrum has a higher baseline compared to spontaneous Raman. There are two likely origins: one is that obtaining spontaneous Raman usually involves a fluorescence background subtraction step, which could potentially remove Raman features that are broad; the other possibility is that SRS spectrum could contain broad features due to two-photon absorption (TPA), a related nonlinear optical process [36]. In order to obtain a chemical map of the different kinds of bead, we use the three SRS spectra as three bases to calculate the "concentration" of the three species at every pixel location with an ordinary least square operation. Figure 3(D) shows the composite (RGB) image of beads based on their calculated concentration, with each color channel corresponding to one species and the intensity corresponding to the "concentration". The beads are well separated with excellent signal-to-noise ratio, even for melamine and PMMA, which are difficult to resolve.

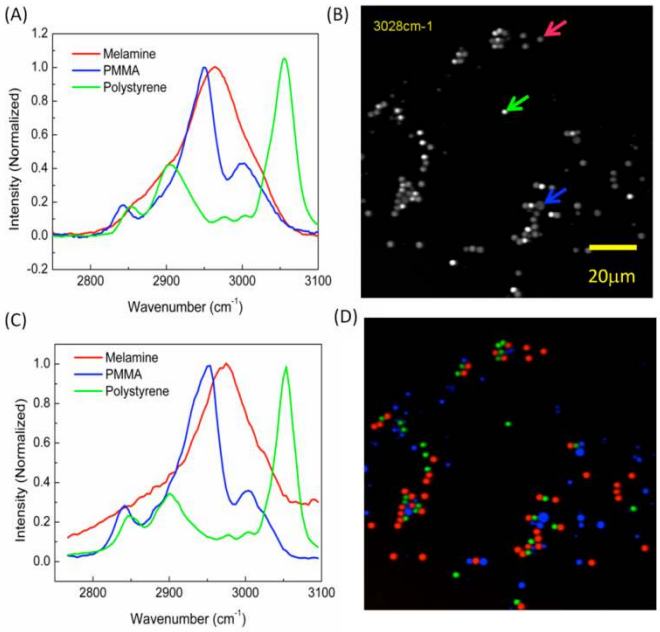

Figure 3: (A) Normalized spontaneous Raman spectra of polymer beads; (B) SRS hyperspectral imaging at 3028 cm^{-1}, with different color arrows pointing out three kinds of beads, respectively; (C) Normalized SRS spectra obtained for the three different beads pointed out by the arrows; (D) Color coded beads distribution based on the SRS spectral decomposition.

SRS hyperspectral imaging of fixed HeLa cells. Biological samples are much more complicated both in terms of chemical composition and spatial inhomogeneity. Most of the time, an *in situ* calibration procedure is not possible. Nonetheless, unlike CARS, the SRS signal has a strictly linear dependence on chemical concentration, thus allowing for straightforward spectral unmixing based on *a priori* calibrations similar to fluorescence spectral imaging [37]. We use a simple model of five compounds to analyze the SRS hyperspectral imaging results. Those five compounds include saturated lipids, unsaturated lipids, cholesterol, protein and water. We demonstrate to our knowledge the first high spatial resolution chemical mapping of single mammalian cells using fast hyperspectral SRS imaging. The SRS calibration spectra were acquired using model compounds: DPPC (represents saturated lipids), DOPC (represents unsaturated lipids), cholesterol, BSA (represents protein), and water. Figure 4 (A-B) shows the

spontaneous Raman spectra and SRS Raman basis spectra in the high wavenumber region, respectively. The SRS spectra reflect the same general trend as spontaneous Raman, even though at a reduced spectral resolution. The decreased resolution arises from higher order chirp as well as residual mismatch in linear chirp. These problems could be alleviated through careful manipulation of the chirp using more sophisticated diagnostic tools such as frequency resolved optical grating (FROG) in combination with pulse shaping tools such as a prism pair or a liquid crystal based pulse shaper.

We image paraformaldehyde fixed HeLa cells with a total of 60 frames evenly spaced between 2810 cm^{-1} and 3088 cm^{-1} at 1.12 sec/frame speed. Movie S1(A-B) shows the depth resolved SRS imaging of two HeLa cells at successive Raman shifts obtained by tuning the interpulse delay between the two chirped pulse trains. Figure 4(C) shows a representative SRS frame at 2923 cm^{-1}. As can be seen from the spatial organization, the upper cell is in mitotic phase with the characteristic shape of two spindles pulling apart the chromosomes, while the bottom cell is likely to be in the interphase because it has a visible nucleus and two nucleoli. The contrasts seen in the movie are mostly from variations in protein and lipids concentration. Here we would like to point out that the signal around 2850cm^{-1} and 2950 cm^{-1} are commonly referred to as CH_2 stretching vibration of lipids and CH_3 stretching vibration of proteins. Such a classification could be misleading because lipids still show strong Raman signal at 2950cm^{-1}, as evidenced by both the SRS spectra and the hyperspectral imaging movie. Obviously, the complete spectra scan provides much more detailed information compared to SRS images at a few discrete Raman shifts. At each pixel, a spectrum can be obtained as seen in Figure 4(D). The spectra are then fitted with the five basis spectra in Figure 4(B), resulting in the concentration of each of the five species. We neglect nucleic acids in our analysis because nucleic acid Raman spectra are close to

that of proteins [38]. Consequently, the decomposed protein images also have a major contribution from nucleic acids. This multi-component fitting to the Raman spectra is quite robust as observed by the small error between experimental and fitted spectra. We also observed that the fitting has larger error on the red side of the spectrum for the nucleoli, which could be due to nucleic acids having slightly red shifted spectra compared to protein.

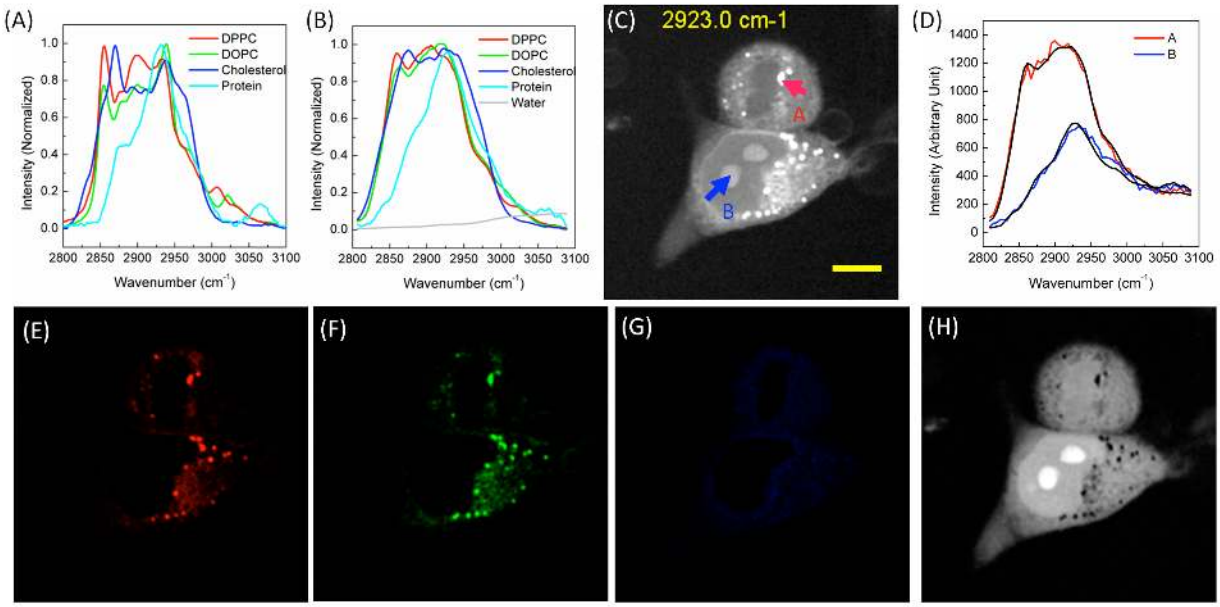

Figure 4: (A) Measured spontaneous spectra of DPPC, DOPC, cholesterol and protein in the CH stretching region; (B) Corresponding SRS calibration spectra for the four macromolecules and water; (C) Hyperspectral imaging frame at 2923 cm^{-1} of two fixed cells; (D) SRS spectra at two individual pixels A, B in (C) and their spectral fitting (black curve) using the five SRS basis spectra; Scale bar: 10μm. (E-H) Nonnegative least square algorithm derived chemical mapping for four macromolecular species: saturated lipids (E), unsaturated lipids (F), cholesterol (G) and proteins (H), respectively. The intensity scales are the same for different colors.

The spectral decomposition results for the four macromolecules are shown in Figure 4(E-H). From the chemical mapping, we can see that the nucleus structure is clearly revealed by negative contrasts in both lipid and cholesterol images. The nucleoli structure is also well resolved in the

protein image as a result of much higher protein/nucleic acid concentration within the nucleoli. This imaging trait could serve as the basis for stain-free digital histopathology. Lipid droplets show up as bright dots, which typically have a size of less than 1 μm. Both saturated lipids and unsaturated lipids are highly localized in the lipid droplets, which are devoid of protein. We also observe that cholesterol has a much more uniform distribution compared to saturated and unsaturated lipids within cellular cytoplasm. It is also less concentrated inside the droplet compared to lipids, suggesting the main chemical component of lipid droplets is triglyceride.

CONCLUSION

In summary, the combination of the high specificity of Raman spectroscopy with the high sensitivity provided by stimulated Raman scattering microscopy allows for excellent capability in label-free imaging based on the intrinsic vibrational contrast of different molecules. The realization of such a powerful combination is obtained through spectral focusing and automated delay scanning. Spectral focusing concentrates most of the optical power into a single Raman vibrational mode, thereby reconciling the bandwidth and resolution conflict and providing a means to optimize the spectral resolution and signal-to-noise ratio. Spectral focusing SRS based on femtosecond lasers should have the same signal size in comparison to its narrowband picosecond SRS counterpart, just like CARS. Considering the shorter pulse duration obtainable with the chirped femtosecond lasers, the sensitivity of our current system can be even higher than narrowband picosecond SRS. Because tuning the delay is simpler, faster and more reliable compared to tuning the laser output wavelength, the spectral focusing approach is a more promising alternative compared to wavelength swept schemes. Moreover, spectral focusing SRS allows easy toggling between spectroscopy mode and imaging mode. We showed that with a

single broadband Ti: sapphire laser, SRS spectroscopy covering fingerprint region can be obtained. Data acquisition speed is mostly limited by the delay line stage movement. In principle, we can achieve submillisecond spectral acquisition using rotating mirrors. This could be a significant advantage over spectral scanning SRS [12,21]. The resolution is currently limited to about 30-40 cm^{-1} due to nonlinear chirp and chirp rate mismatch, worse than that is obtainable with spectral scanning SRS, but it can be improved by larger chirp and by incorporating prism pairs or pulse shapers to correct higher order chirp. We now have spectral scanning SRS and spectral focusing as alternative approaches in obtaining hyperspectral Raman imaging data. Both methods have limitations and advantages. The choice of method could depend to a large extent on the importance of spectral resolution, reliability in spectra acquisition, and imaging speed, as well as the available laser system. With the advent of a dual output femtosecond laser such as the Newport Insight and new femtosecond fiber laser systems, it is very likely that spectral focusing SRS will be a viable approach in hyperspectral Raman study of various biological systems.

We demonstrated fast Raman imaging using spectral focusing SRS approach on both a polymer bead mixture and biological cells. In comparison to similar approaches using CARS imaging, our method has significant advantages. The spectral reproducibility is critical in unmixing convoluted spectra. CARS is known to have a nonresonant background problem, resulting in distorted and irreproducible spectral shape, especially in spatially inhomogeneous samples. Compared to previous implementations of spectral focusing SRS, our approach provides orders of magnitude higher signal-to-noise ratio, enabling an imaging speed that is a thousand times faster. The SRS spectra obtained from different kinds of beads closely resemble their spontaneous Raman spectra, and does not depend on their local environment. In fact, they could be even more reliable that spontaneous Raman because SRS signal has much better

immunity to fluorescence background. With the spectral information, the chemical composition can be extracted using a simple nonnegative least square algorithm, provided that the basis spectra for individual components are known *a priori*. The basis spectra can be obtained *in situ* for spatially segregated samples, as shown in the bead imaging case, or separately measured, as demonstrated in cell imaging. Because the system is over-determined, it is not necessary to obtain the entire spectra. Only discrete steps at locations where there are large variations in spectra need to be imaged. The number of steps, at a minimum, can be the same as the number of species. By doing this the hyperspectral imaging speed can be significantly increased by an order of magnitude. In the high wavenumber region, the signal is usually very strong, and fast imaging can be implemented. It is possible to speed up the imaging to video rate with a suitable scanner, resulting in subsecond high spatial resolution chemical mapping. When the chemical composition is not known *a priori*, it is possible to use multivariate techniques such as principle component analysis to identify important spectral signatures[39,40]. This could be very useful in medical diagnosis based on Raman hyperspectral imaging. We believe that SRS hyperspectral imaging is a powerful approach in studying inhomogeneous systems such as tissue. Future development will focus on improving spectral resolution, extending imaging into the fingerprint region, and applying fast SRS imaging technology to study lipid metabolism and tissue diagnosis.

Note added: While this manuscript is under review, a paper on video-rate hyperspectral SRS imaging based on the spectral scanning approach is published [41].

ASSOCIATED CONTENT

Supporting Information. Detailed descriptions of experimental setup, data analysis and high resolution imaging results are available free of charge via the Internet at http://pubs.acs.org.

AUTHOR INFORMATION

Corresponding Author

xie@chemistry.harvard.edu

Author contributions

D.F. and X.S.X. conceived the experiment. D.F., G.H., C.F. and X.Z. performed the experiments. D.F. and X.S.X wrote the manuscript.

ACKNOWLEDGEMENT

This paper is dedicated to the memory of Paul Barbara. We thank Dr. Christof Gebhardt for providing the HeLa cells. This spectroscopy work was supported by the U.S. Department of Energy's Basic Energy Sciences Program (DE-FG02-09ER16104), while the biological applications were supported by the NIH T-R01 (1R01EB010244-01) award to X.S.X.

REFERENCES:

(1) Chan, J. W.; Taylor, D. S.; Zwerdling, T.; Lane, S. M.; Ihara, K.; Huser, T. *Biophys. J.* **2006**, *90*, 648-656.

(2) van Manen, H.-J.; Kraan, Y. M.; Roos, D.; Otto, C. *Proceedings of the National Academy of Sciences of the United States of America* **2005**, *102*, 10159-10164.

(3) Baena, J. R.; Lendl, B. *Current Opinion in Chemical Biology* **2004**, *8*, 534-539.

(4) Zumbusch, A.; Holtom, G. R.; Xie, X. S. *Physical Review Letters* **1999**, *82*, 4142-4145.

(5) Cheng, J. X.; Xie, X. S. *J. Phys. Chem. B* **2004**, *108*, 827-840.

(6) Evans, C. L.; Potma, E. O.; Puoris'haag, M.; Cote, D.; Lin, C. P.; Xie, X. S. *Proceedings of the National Academy of Sciences of the United States of America* **2005**, *102*, 16807-16812.

(7) Muller, M.; Schins, J. M. *J. Phys. Chem. B* **2002**, *106*, 3715-3723.

(8) Kano, H.; Hamaguchi, H. *Opt. Express* **2005**, *13*, 1322-1327.

(9) Cheng, J.-x.; Volkmer, A.; Book, L. D.; Xie, X. S. *J. Phys. Chem. B* **2002**, *106*, 8493-8498.

(10) Volkmer, A. *Journal of Physics D-Applied Physics* **2005**, *38*, R59-R81.

(11) Lin, C. Y.; Suhalim, J. L.; Nien, C. L.; Miljkovic, M. D.; Diem, M.; Jester, J. V.; Potma, E. O. *J. Biomed. Opt.* **2011**, *16*, 021104-9.

(12) Garbacik, E. T.; Herek, J. L.; Otto, C.; Offerhaus, H. L. *Journal of Raman Spectroscopy* **2012**, *43*, 651-655.

(13) Hellerer, T.; Enejder, A. M. K.; Zumbusch, A. *Appl. Phys. Lett.* **2004**, *85*, 25-27.

(14) Cicerone, M. T.; Aamer, K. A.; Lee, Y. J.; Vartiainen, E. *Journal of Raman Spectroscopy* **2012**, *43*, 637-643.

(15) Freudiger, C. W.; Min, W.; Saar, B. G.; Lu, S.; Holtom, G. R.; He, C.; Tsai, J. C.; Kang, J. X.; Xie, X. S. *Science* **2008**, *322*, 1857-1861.

(16) Saar, B. G.; Freudiger, C. W.; Reichman, J.; Stanley, C. M.; Holtom, G. R.; Xie, X. S. *Science* **2010**, *330*, 1368-1370.

(17) Nandakumar, P.; Kovalev, A.; Volkmer, A. *New. J. Phys* **2009**, *11*, 033026.

(18) Ozeki, Y.; Dake, F.; Kajiyama, S. i.; Fukui, K.; Itoh, K. *Opt. Express* **2009**, *17*, 3651-3658.

(19) Saar, B. G.; Zeng, Y.; Freudiger, C. W.; Liu, Y.-S.; Himmel, M. E.; Xie, X. S.; Ding, S.-Y. *Angew. Chem.* **2010**, *122*, 5608-5611.

(20) Wang, M. C.; Min, W.; Freudiger, C. W.; Ruvkun, G.; Xie, X. S. *Nat. Meth.* **2011**, *8*, 135-138.

(21) Suhalim, J. L.; Chung, C.-Y.; Lilledahl, M. B.; Lim, R. S.; Levi, M.; Tromberg, B. J.; Potma, E. O. *Biophys. J.* **2012**, *102*, 1988-1995.

(22) Ploetz, E.; Laimgruber, S.; Berner, S.; Zinth, W.; Gilch, P. *Appl. Phys. B* **2007**, *87*, 389-393.

(23) Lu, F.-K.; Ji, M.; Fu, D.; Ni, X.; Freudiger, C. W.; Holtom, G.; Xie, X. S. *Mol. Phys.* **2012**, *110*, 1927-1932.

(24) Freudiger, C. W.; Min, W.; Holtom, G. R.; Xu, B.; Dantus, M.; Sunney Xie, X. *Nat. Photon.* **2011**, *5*, 103-109.

(25) Fu, D.; Lu, F. K.; Zhang, X.; Freudiger, C.; Pernik, D. R.; Holtom, G.; Xie, X. S. *Journal of the American Chemical Society* **2012**, *134*, 3623-3626.

(26) Andresen, E. R.; Berto, P.; Rigneault, H. *Opt. Lett.* **2011**, *36*, 2387-2389.

(27) Beier, H. T.; Noojin, G. D.; Rockwell, B. A. *Opt. Express* **2011**, *19*, 18885-18892.

(28) Potma, E. O.; Mukamel, S. In *Coherent Raman Scattering Microscopy*; Cheng, J.-X., Xie, X. S., Eds.; CRC Press: 2012.

(29) Zhang, D.; Slipchenko, M. N.; Cheng, J.-X. *The Journal of Physical Chemistry Letters* **2011**, *2*, 1248-1253.

(30) Knutsen, K. P.; Johnson, J. C.; Miller, A. E.; Petersen, P. B.; Saykally, R. J. *Chemical Physics Letters* **2004**, *387*, 436-441.

(31) Pegoraro, A. F.; Ridsdale, A.; Moffatt, D. J.; Jia, Y.; Pezacki, J. P.; Stolow, A. *Opt. Express* **2009**, *17*, 2984-2996.

(32) Rocha-Mendoza, I.; Langbein, W.; Borri, P. *Appl. Phys. Lett.* **2008**, *93*, 201103-3.

(33) Chen, B.-C.; Sung, J.; Wu, X.; Lim, S.-H. *J. Biomed. Opt.* **2011**, *16*, 021112-8.

(34) Holtom, G. R. *Opt. Lett.* **2006**, *31*, 2719-2721.

(35) Okuno, M.; Kano, H.; Leproux, P.; Couderc, V.; Day, J. P. R.; Bonn, M.; Hamaguchi, H.-o. *Angew. Chem. Int. Ed.* **2010**, *49*, 6773-6777.

(36) Fu, D.; Ye, T.; Matthews, T. E.; Chen, B. J.; Yurtserver, G.; Warren, W. S. *Optics Letters* **2007**, *32*, 2641-2643.

(37) Zimmermann, T.; Rietdorf, J.; Pepperkok, R. *FEBS Letters* **2003**, *546*, 87-92.

(38) Nijssen, A.; Maquelin, K.; Santos, L. F.; Caspers, P. J.; Schut, T. C. B.; den Hollander, J. C.; Neumann, M. H. A.; Puppels, G. J. *J. Biomed. Opt.* **2007**, *12*, 034004-7.

(39) Pohling, C. *J. Biomed. Opt.* **2011**, *16*, 021105.

(40) Miljkovic, M.; Chernenko, T.; Romeo, M. J.; Bird, B.; Matthaus, C.; Diem, M. *Analyst* **2010**, *135*, 2002-2013.

(41) Ozeki, Y.; Umemura, W.; Otsuka, Y.; Satoh, S.; Hashimoto, H.; Sumimura, K.; Nishizawa, N.; Fukui, K.; Itoh, K. *Nat. Photon.* **2012**, *6*, 845-851.

TOC figure

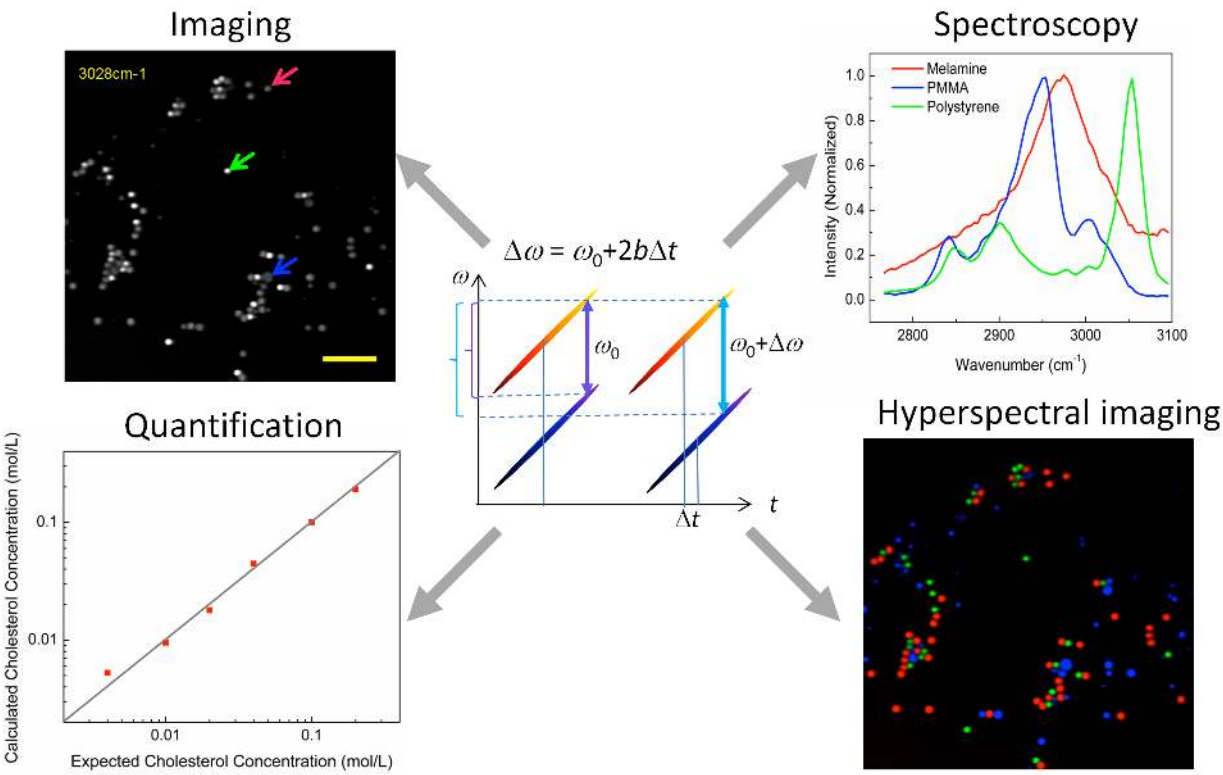
Imaging
3028cm-1
Spectroscopy
Melamine
PMMA
Polystyrene
Intensity (Normalized)
Wavenumber (cm-1)
Δω = ω0+2bΔt
ω
ω0
ω0+Δω
t
Δt
Quantification
Calculated Cholesterol Concentration (mol/L)
Expected Cholesterol Concentration (mol/L)
Hyperspectral imaging